Radio-interferometric Object Trajectory Estimation

Gergely Zachár and Gyula Simon
Department of Computer Science and Systems Technology, University of Pannonia, Veszprém, Hungary

Keywords: Sensor Network, Localization, Tracking, Radio-Interferometry.

Abstract: In this paper a novel radio-interferometric object trajectory estimation method is proposed, which can be used to track moving objects. The system utilizes a low number of fixed infrastructure nodes equipped with radio transceivers, and the tracked object also carries a simple transceiver. Selected transmitter infrastructure nodes produce interference signals at the fixed infrastructure receivers and the tracked receiver. Transmitter and receiver roles are rotated, thus multiple interference signals are produced, which is measured by synchronized receiver pairs. Measurements are then compared to pre-computed phase maps while the object is moving. During object movement the system resolves position ambiguities and the exact object trajectory is determined. The performance of the proposed method is illustrated by simulation examples and real measurements.

1 INTRODUCTION

Object localization and object tracking is an important functionality in many applications and thus various approaches have been proposed, including image processing, acoustic, and RF-based solutions.

Image- and video-based solutions extract significant visual information from the frames and thus can find and follow objects along a series of frames. This approach can be used for object detection, identification, localization, and tracking, see e.g. (Comaniciu, 2003). In acoustic ranging methods the time of flight of acoustic signals (mainly ultrasound) is measured, and the system determines pairwise distances between nodes with known and unknown locations, and from the pairwise distance set it calculates the unknown positions, see e.g. (Ajdler, 2004).

Among the RF-based solutions GPS is the most widespread solution in applications where line of sight to satellite can be provided. In indoor applications, however, alternative methods are searched. Positioning based on signal strength is probably the simplest of RF-based methods, and can provide a few meters of accuracy, with sufficiently dense transmitter infrastructure and an *a priori* measured reference map (Au, 2012). Time of flight of RF signals can also be used for ranging, using a significantly more sophisticated system (Schwarzer, 2008). To avoid high precision time of flight measurements, (Maroti, 2005) proposed radio interferometric measurements and a corresponding localization method, which can work with inexpensive hardware and software solutions.

In this paper a novel object tracking method will be proposed, which utilizes radio-interferometric measurements. In contrast to the former localization method of (Maroti, 2005), the proposed solution is not suitable for localization but for tracking. The proposed solution is either able to determine the full track of a moving object if the object has covered a sufficiently large trajectory, or can follow the trajectory of an object if its original position is known. The proposed solution also has much lower requirement in terms of measurement precision, than the former method of (Maroti, 2005).

In Section 2 radio interferometric positioning is reviewed, the basic elements of which will be heavily utilized in the proposed solution. In Section 3 the proposed solution is introduced. Section 4 present the evaluation of the proposed solution, using simulations and real measurements. Section 5 presents open questions, possible enhancements, and concludes the paper.

2 RELATED WORK

Radio Interferometric Positioning (RIPS) was

Zachár G. and Simon G..
Radio-Interferometric Object Trajectory Estimation.
DOI: 10.5220/0004836002680273
In *Proceedings of the 3rd International Conference on Sensor Networks* (SENSORNETS-2014), pages 268-273
ISBN: 978-989-758-001-7

proposed by (Maroti, 2005), utilizing inexpensive off the shelf components and simple signal processing methods, allowing the creation of low cost positioning systems using sensor networks. Instead of high frequency signal processing, RIPS utilizes low frequency interference signals, produced by the interference of two radio signals, having approximately the same carrier frequency. The schematics of the radio interferometric measurement are shown in Figure 1. In the measurement process two transmitters (A and B) are used, which transmit only carrier signals (sine waves) with frequencies f_A and f_B, respectively. The carrier frequencies are set to be close to each other, thus a low frequency interference signal is produced at two receivers, denoted by C and D in Figure 1. The frequency of the interference signal is $\Delta f = |f_A - f_B|$ at both receivers, but its phase depends on the relative positions of the transmitters and the receivers. This phase difference is used to provide position estimates.

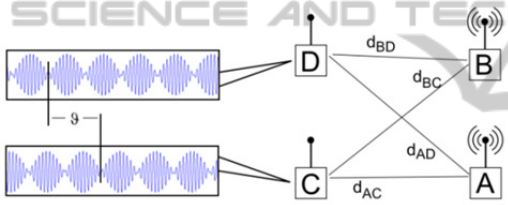

Figure 1: Radio interferometric measurements.

Note that the interference signal is actually the received signal strength (RSSI), which can be measured in most RF transceivers. By providing time synchronization between receivers C and D, the phase difference ϑ between the RSSI signals of the receivers can be measured. The phase difference ϑ can be expressed as a function of the relative positions of the transceivers and receivers, as follows:

$$\vartheta(f) = 2\pi \frac{d_{ABCD}}{c/f} \ (mod\ 2\pi) \qquad (1)$$

where f is the carrier frequency ($f \approx f_A \approx f_B$), c is the speed of light, the pairwise distances d_{AC}, d_{AD}, d_{BC}, and d_{BD} are defined in Figure 1, and the quantity d_{ABCD} is the following linear combination of the pairwise distances:

$$d_{ABCD} = d_{AD} - d_{BD} + d_{BC} - d_{AC}. \qquad (2)$$

Note that in (1) the phase values are wrapped, ($0 \leq \vartheta < 2\pi$), thus the exact value of d_{ABCD} cannot be expressed from a single phase measurement. In (Maroti, 2005) the phase ambiguity problem is addressed by using multiple carrier frequencies, providing multiple $\vartheta(f)$ measurements. Solving Diophantine equations of $\vartheta(f)$ values the exact value of d_{ABCD} can be calculated. The proposed method in (Maroti, 2005) works well if the error of ϑ is small, thus RIPS required long measurements (80 minutes of data collection time was reported in (Maroti, 2005)).

In our proposed solution we do not try to resolve the phase ambiguity problem at one position, rather we use only the wrapped phase values and resolve the ambiguity problem with multiple measurements at different positions, as the object moves. Thus the proposed solution is suitable for tracking, but not for localization.

3 PROPOSED SOLUTION

The proposed solution offers two operation modes:

Mode 1: on-line tracking of objects with *known* initial position. In this mode the movement of the object is tracked in real-time from the known initial position.

Mode 2: off-line tracking of objects with *unknown* initial position. In this mode a sufficiently long data must be recorded, while the object moves; after sufficient amount of data is collected the full object track is determined (retroactively) and the tracking can be continued as in on-line Mode 1.

Since Mode 1 is a subcase of Mode 2, we will discuss only the operation of Mode 2 in detail.

3.1 Requirements

The proposed solution has some realistic assumptions and requirements, as follows:

R1: The exact positions of the infrastructure nodes are known.

R2: The movement of the object is slow, compared to the sampling frequency. According to experiments, the object should not move more than a few tens of millimeters between two consecutive phase measurement rounds.

R3: The object trajectory is long enough to allow the resolution of the ambiguity problems (Mode 2 only). There is no explicit known formula yet on how long the trajectory should be; according to our experiments the more complex the movement (containing multiple directions) the shorter trajectory is enough. See the simulations and the measurement result is Section 4.

R4: The initial object position must be known (Mode 1 only). In Mode 2 the initial position is

unknown and is determined by the algorithm.

3.2 Tracking Infrastructure

The tracking infrastructure contains transceivers at known positions, which can either play the role of transmitters to generate interference signals at the receivers, or receivers to allow phase difference measurements, as described in Section 2. The tracked node is always a receiver. Infrastructure nodes alter their roles, thus different interference signals can be generated.

A simple measurement uses three infrastructure nodes (two transmitters and one receiver) and the tracked receiver node, in a measurement configuration. The four nodes in the configuration can measure a phase difference value ϑ, which depends on the positions of both the infrastructure nodes and the tracked node. Such simple measurements are carried out with different configurations, to provide a measurement round, containing C simple measurements. The measurement results of a complete round will be used as inputs in each step of the tracking algorithm.

Figure 2 illustrates a scenario with four fixed nodes A, B, C, D, and one tracked node X. In this case $C_{max} = 12$ possible configuration exists, as shown in the table of Figure 2.

3.3 Position Confidence Map

In each configuration c $(c = 1, 2, \dots, C)$ the ideal phase values $\vartheta_c^{(id)}(p)$ can be calculated for every possible object position p, using (1) and (2). For two dimensions, this gives a 2D phase map. Note that phase maps can be pre-computed and stored, to increase the speed of the algorithm.

Measurement round k produces C phase measurements, each measurement corresponding to one measurement configuration, as follows:

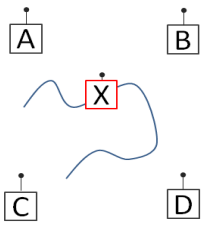

Config	A	B	C	D	X
C1	T	T	R		R
C2	T	R	T		R
C3	T	R		T	R
C4	R	T	T		R
C5	R	T		T	R
C6	R		T	T	R
C7	T	T		R	R
...					
C12		R	T	T	R

Figure 2: An example tracking infrastructure with for fixed nodes (A, B, C, D) and one tracked node (X). The possible configurations are listed in the table.

$$\vartheta_{meas}(k) = [\vartheta_1(k), \vartheta_2(k), \dots, \vartheta_C(k)] \quad (3)$$

Using the ideal phase maps and the measurements, a phase offset is calculated for each scenario c, as follows:

$$\Delta\vartheta_c(p,k) = \min_{i=-1,0,1} \left|\vartheta_c^{(id)}(p) + i2\pi - \vartheta_c(k)\right| \quad (4)$$

Note that the phase offset values $\Delta\vartheta_c$ are between 0 and π. From the phase offsets an error map is calculated, as follows:

$$\varepsilon(p,k) = \frac{1}{C\pi^2}\sum_{c=1}^{C}\left(\Delta\vartheta_c(p,k)\right)^2 \quad (5)$$

The error ε is zero if the measurements exactly correspond to the ideal values; and the maximum error is 1, indicating large difference between the ideal and measured phase values. Thus from the error map a confidence map can be defined, as follows:

$$\beta(p,k) = 1 - \varepsilon(p,k) \quad (6)$$

Confidence value $\beta(p,k)$ close to one indicates that position p can indeed be the real object position in time instant k, while low confidence values show that it is unlikely that the object is in position p in time instant k.

Figure 3 shows a confidence map computed for a scenario similar to the one shown in Figure 2. The true object position is at the center of the figure. Figure 3(a) shows the case when there is no measurement noise; in this case there are significant and sharp peaks in the confidence map. Note that in this case the confidence value is exactly 1 at the true object position, but there are several other significant peaks at phantom positions. This phenomenon is due to the phase wrapping in (1), and thus the true object position cannot be determined from one measurement. The noisy case is shown in Figure 3 (b), where the peaks are less high and somewhat blurred. The phantom positions are clearly observable here as well.

An important observation, which is the basis of the proposed algorithm, is the following: the true object location has high confidence value all along the track of the object (exactly one in noiseless case, and close to one in noisy case). The phantom positions, however, change their confidence values, as the object moves along its trajectory. This phenomenon is quite salient when a series of confidence maps is observed: the peak, corresponding to the true object position, is moving along the object trajectory; at the same time the phantom peaks fade and new phantoms appear, only

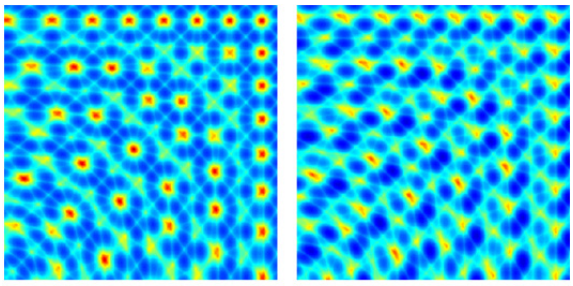

Figure 3: Calculated confidence map for (a) noise free and (b) noisy measurements. Red colors show high confidence values, dark blue denotes low confidence values. The true position is at the center, the other peaks represent phantom positions.

few phantoms living longer than a few meters.

The phenomenon is illustrated in Figure 4, where the confidence values, corresponding to the true and a phantom position, are denoted by red and blue lines, respectively. Note that in noisy case the confidence value of a phantom position may be higher than that of the true position. The phantom's confidence, however, will eventually decrease. Thus the tracking algorithm monitors the (true or phantom) trajectories, and keeps only those, which have steadily high confidence values.

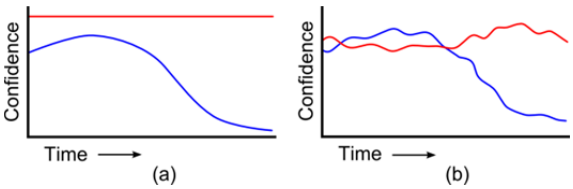

Figure 4: Illustration of phase confidence values at the real (red line) and a phantom (blue line) position of a moving object, as a function of time. (a) ideal, noise free case, (b) noisy case.

3.4 Tracking Algorithm

The input of the tracking algorithm in each time instant k $(k = 1, 2, \dots, N)$ is the measured phase vector $\vartheta_{meas}(k)$, where the vector contains C phase measurements, corresponding to the utilized configurations, see (3). The output of the algorithm is the actual track list (*atrack*), which ideally contains one and only one track. At the beginning of the algorithm several possible starting points are identified: the true one and many phantoms. As the object moves and new measurements are available, the algorithm checks whether the current tracks can be continued, according to the new measurements, or not. A track can be continued if a possible location (true or phantom) is close enough to the end of the track. The required maximum distance is defined in variable *limit*. Tracks which cannot be continued (thus proved to be phantom tracks) are removed from the actual track list and are stored in list *phtrack*. The list of the actual tracks is thus shrinking, as the moving object provides more and more information to resolve ambiguities, and finally contains only the true track alone. The pseudo-code of the algorithm is the following:

```
input: ϑ_meas(k), k=1..N
output: atrack, phtrack
Initialization:
atrack = {}
phtrack = {}
map = confidence_map(ϑ_meas(1))
points = possible_positions(map)
for each p ∈ points
   t= new Track
   t.add(p)
   atrack = atrack ∪ t

Tracking:
for each ph ∈ ϑ_meas(2..n)
   map = confidence_map(ph)
   points = possible_positions(map)
   for each t ∈ atrack
      [d, p] =
      min_distance(t.last_point, points)
      if d < limit
         t.add(p)
      else
         atrack = atrack \ t
         phtrack = phtrack ∪ t
```

The helper functions in the algorithm are the following:

`confidence_map(phase_values)`: calculates the confidence map for a given phase measurement set, corresponding to one time instant. See Figure 3. for illustration of a confidence map.

`possible_positions(map)`: analyses the confidence map and determines possible positions. In the current implementation we use a hard threshold *confmin* to select the high peaks in the map, then a blob analysis is run to determine the connected areas, finally the center of each area is selected as possible position.

`min_distance(p, pv)`: from a vector of points *pv* selects the closest point to a point *p*. Returns both the closest point and the distance.

4 EVALUATION

In this section the proposed method will be evaluated using simulations and real measurements. In the simulations and the real measurements a 4-by-4 meter area was used where the four infrastructure nodes were placed into the corners, i.e. the fixed nodes were placed at positions (0, 0), (0, 4), (4, 0), and (4, 4), respectively. In all the experiments six configurations were used, corresponding to configurations C1…C6 in Figure 2.

First a simulated moving object will be tracked using various levels of phase measurement error. Then a proof-of-concept tracking test will be presented using real measurements.

4.1 Tracking Simulations

The proposed algorithm was tested with a simulated object trajectory, which started from position (1, 1), moved to (3, 3) and then moved to (3, 1). To the ideal phase values various amount of additive phase noise was added to simulate noisy measurements. In the two experiments zero-mean normal distribution noise was used with $\sigma = 0.1\pi$ and $\sigma = 0.2\pi$, respectively. In both simulations parameters *confmin* and *limit* were set to 0.8 and 0.1m, respectively.

The results of the tests can be seen in Figure 5, where red lines represent the identified true object track, while blue lines show the phantom trajectories. Blue dots show the starting track positions.

As can be seen in Figure 5, from the initial tracking positions phantom tracks of various lengths were detected. Note that the directions of the real and phantom tracks were approximately the same. Also note that in the noisier simulation the phantom tracks are much shorter, because the same *confmin* threshold for lower confidence values (see Section 4.1) results an earlier abortion of phantom tracks.

The length of the true trajectory is $N = 400$. With $\sigma = 0.1\pi$ the five longest phantom tracks have 285, 228, 116, 108, and 98 points, while with $\sigma = 0.2\pi$ their corresponding lengths are 35, 35, 25, 19, and 19 points. The number of starting points somewhat decreased in the noisier experiment from 164 to 143. This is again due to the fact that fewer initial points exceeded the same confidence limit.

The accuracy of the position estimation was also evaluated in the simulations. In the $\sigma = 0.1\pi$ case the maximum, average and the standard deviation of the estimation error are 25.2mm, 8.3mm, and 18.6mm, respectively. In the $\sigma = 0.2\pi$ case the maximum, average and the standard deviation of the estimation error increased to 59.9mm, 17.0mm, and 19.1mm, respectively.

4.2 Measurement Results

To test the proposed method a real measurement was also performed. The used special dual-radio nodes are based on Atmel's ATmega128RFA1 microcontroller, equipped with an integrated 2.4GHz transceiver. The other radio chip is a Silicon Lab's Si4432 transceiver, which was used for the radio interferometric measurements. During the measurements we used the 868 MHz ISM frequency band and fine-tuned the radios with the available 312,5 Hz accuracy. The synchronized receivers performed phase difference measurement on the RSSI data, sampled with frequency of 62.5 kHz.

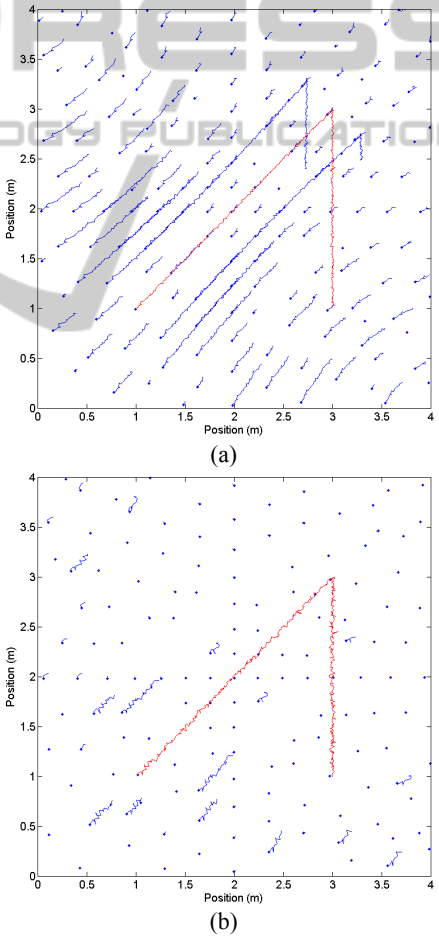

(a)

(b)

Figure 5: Simulation result with various measurement phase noise. The standard deviation of the additive noise was (a) $\sigma = 0.1\pi$ and (b) $\sigma = 0.2\pi$. Active and phantom object trajectories are shown with red and blue lines, respectively. Blue dots present the initial starting positions of the tracks.

In the test, shown in Figure 6, four nodes and six configurations were used, as was described at the beginning of Section 4. Each of the devices were placed 1.25m above ground level and the tracked node was carried in hand by a person. The test took 50 seconds while 271 rounds were measured (altogether 1626 phase measurements were performed).

The tracking algorithm was executed with parameter values of *limit* = 0.1m, and *confmin* = 0.6. Initially 169 possible locations were found.

The length of the actual track is 271, as shown in Figure 6, with red line. The longest five phantom tracks have lengths of 86, 71, 69, 69, and 69 steps.

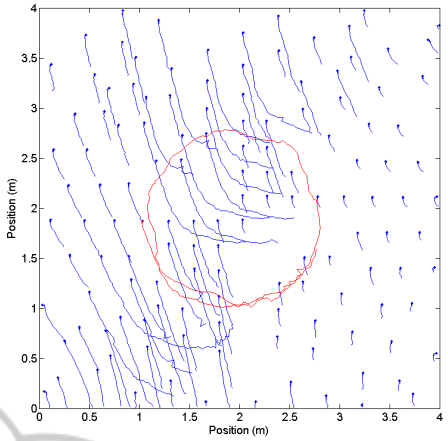

Figure 6: Output of the tracking algorithm based on a real measurement. The computed real object track is shown by red line, while the phantom tracks are shorter blue lines. The initial track positions are denoted by blue dots.

4 CONCLUSIONS

In this paper a novel radio-interferometric object tracking method was proposed. In contrast to former radio-interferometric localization methods, the proposed solution resolves the location ambiguity while the object is moving and provides more and more measurements.

The proposed solution is able to determine the full track of a moving object, after the object has covered a sufficiently large trajectory. Alternatively it can follow the trajectory of an object in real time, if the original position of the object is known.

The performance of the algorithm was tested in simulations and real measurements. The proposed method, according to simulation experiments, is robust when the measurement noise is moderate. The algorithm performed also well in a measurement using prototype equipment.

Although the preliminary results are very promising there are several open questions. It is not known yet how long trajectory the object should cover before all ambiguities can be resolved. The dependence of the minimal trajectory length on various system parameters is also unknown. The current measurement rate (approximately 5 rounds per second) should also be improved to allow tracking of faster objects.

Possible improvements include acceleration of confidence map generation with GPU based parallel computing. Currently a simple image processing algorithm is used to identify the possible locations; with a tailor-made adaptive algorithm the performance of the algorithm possibly can be improved. The robustness of the tracking can also be increased using model based approaches e.g. Kalman-filtering.

ACKNOWLEDGEMENTS

This research was supported by the Hungarian Government and the European Union and co-financed by the European Social Fund under projects TÁMOP-4.2.2.A-11/1/KONV-2012-0073 and TÁMOP-4.2.2.C-11/1/KONV-2012-0004. Gergely Zachár was supported by the European Union and co-financed by the European Social Fund in the framework of TÁMOP 4.2.4. A/2-11-1-2012-0001 'National Excellence Program'.

REFERENCES

Ajdler, T., Kozintsev, I., Lienhart, R., Vetterli, M., 2004. Acoustic source localization in distributed sensor networks. In *Conference Record of the Thirty-Eighth Asilomar Conference on Signals, Systems and Computers*, Vol.2, pp.1328-1332.

Au, A. W. S., et al, 2012. Indoor Tracking and Navigation Using Received Signal Strength and Compressive Sensing on a Mobile Device. IEEE Transactions on Mobile Computing, Aug. 2012.

Comaniciu, D., Ramesh, V., Meer, P., 2003. Kernel-based object tracking. IEEE Trans. Patt. Analy. Mach. Intell. 25, pp. 564–575.

Maroti M., et al, 2005. Radio Interferometric Geolocation. In *ACM Third International Conference on Embedded Networked Sensor Systems (SenSys 05)*, San Diego, CA, pp. 1-12.

Schwarzer, S., Vossiek, M., Pichler, M., Stelzer, A., 2008. Precise distance measurement with IEEE 802.15.4 (ZigBee) devices. In *2008 IEEE Radio and Wireless Symposium*, pp.779-782.